Contrasting response of European forest and grassland energy exchange to heatwaves

Reference:
Teuling Adriaan J., Seneviratne Sonia I., Stöckli Reto, Reichstein Markus, Moors Eddy, Ciais Philippe, Luyssaert Sebastiaan, van den Hurk Bart, Ammann Christof, Bernhofer Christian, ...- Contrasting response of European forest and grassland energy exchange to heatwaves
Nature geoscience - ISSN 1752-0894 - 3:10(2010), p. 722-727
Full text (Publisher's DOI): https://doi.org/10.1038/NGEO950
To cite this reference: https://hdl.handle.net/10067/853690151162165141

Contrasting response of European forest and grassland energy exchange to heatwaves

Adriaan J. Teuling[1,2], Sonia I. Seneviratne[1], Reto Stöckli[3], Markus Reichstein[4], Eddy Moors[5], Philippe Ciais[6], Sebastiaan Luyssaert[6], Bart van den Hurk[7], Christof Ammann[8], Christian Bernhofer[9], Ebba Dellwik[10], Damiano Gianelle[11], Bert Gielen[12], Thomas Grünwald[9], Katja Klumpp[13], Leonardo Montagnani[14,15], Christine Moureaux[16], Matteo Sottocornola[11], Georg Wohlfahrt[17], and FLUXNET members[18]

[1] *Institute for Atmospheric and Climate Science, ETH Zurich, Switzerland*

[2] *Department of Environmental Sciences, Wageningen University, The Netherlands*

[3] *MeteoSwiss, Zurich, Switzerland*

[4] *Max-Planck Institute for Biogeochemistry, Jena, Germany*

[5] *Alterra, Wageningen, The Netherlands*

[6] *Laboratoire des Sciences du Climat et de l'Environnement, LSCE, Gif-sur-Yvette, France*

[7] *KNMI, De Bilt, The Netherlands*

[8] *Agroscope ART, Zurich, Switzerland*

[9] *Department of Hydrosciences, TU Dresden, Germany*

[10] *Risø National Laboratory for Sustainable Energy, Technical University of Denmark, Roskilde, Denmark*

[11] *IASMA Research and Innovation Centre, Fondazione E. Mach,*
Environment and Natural Resources Area, Trento, Italy

[12] *Department of Biology, University of Antwerp, Belgium*

[13] *INRA, Grassland Ecosystem Research (UREP), Clermont-Ferrand, France*

[14] *Forest Services and Agency for the Environment, Bolzano, Italy*

[15] *University of Bozen-Bolzano, Faculty of Sciences and Technology, Bolzano, Italy*

[16] *Gembloux Agro-Bio Tech, University of Liège, Gembloux, Belgium*

[17] *Institute of Ecology, University of Innsbruck, Innsbruck, Austria*

[18] *www.fluxdata.org/DataInfo/default.aspx*

Recent European heatwaves have raised interest in the impact of land cover conditions on temperature extremes. It is currently believed that such extremes are enhanced by stronger surface heating of the atmosphere induced by below-average soil moisture conditions. However, the impact of land cover on exchanges of water and energy and its interaction with the soil water balance during heatwaves is largely unknown. Here we show that observations from an extensive network of flux towers in Europe reveal a contrasting temporal response between forest and grassland ecosystems during heatwaves. Initially, surface heating is twice as high over forest than over grassland, where it is suppressed by increased evaporation in response to increased solar radiation and temperature. Ultimately, however, this process accelerates soil moisture depletion over grassland and induces a critical shift in the regional climate system leading to increased heating, a mechanism that may explain the extreme temperatures in August 2003. Thus, the conservative water use of forest contributes to increased temperatures in the short term, but mitigates the impact of the most extreme hot and/or long-lasting events. We anticipate our study to provide a new perspective on the relation between land cover, the hydrological cycle, and regional climate extremes.

Climate extremes, such as prolonged periods of above-average high temperatures, have a large societal and economic impact. In Central and Western Europe, both average summer temperatures and heatwave occurrence are projected to increase in the coming decades [1,2,3,4], associated with a transition towards a dryer summer climate regime [2]. Trends in past decades are consistent with these projections [5]. Large-scale, record-breaking summer heatwaves occurred recently in 2003 [1,6,7,8] and 2006 [9], associated with widespread ecosystem damage and crop failures, increased human mortality, and water shortages

[1,10,11,7,12]. European heatwaves are favoured by two atmospheric circulation patterns [13]: a deep anomalous trough covering the North Atlantic (June 2003 [13]), and an Omega Blocking situation with an extensive high located over Northern Europe (August 2003 [13], July 2006 [9], see Supplementary Figure 1). Model simulations and heat budget analyses suggest that the warm conditions associated with these circulation patterns can be amplified by reduced evaporative cooling due to soil moisture depletion [11,2,6,14]. However, the relation between land cover and the temporal dynamics of evapotranspiration (hereafter evaporation) and its impact on temperature during heatwave days (HWDs, see Methods) remain to be quantified.

Land use-related variations in surface exchanges have the potential to impact local climate [15,16], but the direction of this effect on global climate is uncertain [17,18,19,20]. It has been suggested that short herbaceous (perennial) vegetation and forest respond differently to conditions typical for HWDs [8,21]. While forest evaporation generally exceeds that of grassland on annual timescales [22], guard cells around stomata may have evolved different strategies to cope with drought conditions that often accompany heatwaves [23]. The strong regulation of stomatal opening in response to radiation, temperature and vapour pressure deficit [21,24,25,26] and the larger rooting depth [27] likely contribute to the conservative character and persistence of forest evaporation [28,29]. Thus, whereas grassland evaporation might exceed forest evaporation at times of ample soil moisture [17,30], the reverse is likely to occur under low soil moisture conditions [31,32,8]. As a result, it is uncertain whether most heating during HWDs takes place over forest or grassland [8,30].

Energy exchange under normal summer conditions

We first analyse the flux partitioning in central-western Europe under normal summer conditions based on observations from a network of eddy covariance flux towers [33]. We selected only towers where temperature and precipitation fall within the range of maritime temperate (Cfb) or hemiboreal (Dfb) climates and where flux climatologies could be estimated from at least two years of observations (Fig. 1a, see Methods and Supplementary Table 1 for site characteristics and references). The towers sample the actual land use distribution, hence our results include the possible impact of co-varying (sub)surface characteristics. The summer (June–August) climatology is calculated over all available years in the period 1997–2008 (but excluding 2003 and July 2006). We focus on a four-hour period (9:00–13:00 UTC) during which heating at the land surface is maximum and controls the magnitude of the diurnal temperature peak (note that there is a phase-shift between the diurnal cycles of heating and temperature). Figure 1b shows the main radiation and energy balance terms for grass-/cropland and forest sites. Median values are shown to minimize the impact of outliers. The terms do not balance due to different data gaps in the radiation and flux terms. Large differences exist in reflected shortwave and net radiation (48 and 49 W m^{-2}, respectively, with forest absorbing more incoming shortwave radiation [31]). Forest emits 40 W m^{-2} more sensible heat (H). The lack of measured energy balance closure is larger over forest (30%) than grassland (19%). This range is consistent with previous findings [31,34,35] and is primarily caused by underestimation of heat exchange by the eddy covariance technique [36,37,38]. The difference in closure (55 W m^{-2}) may be partly attributed to larger heat storage in forest between the land surface and the eddy covariance sensor [31,39,35], which is implicitly included in the closure residual term (ε), as well as greater flow distortion errors on the sonic anemometer vertical velocity [38,40].

Energy exchange under heatwave conditions

During HWDs, the measured energy balance residual improves to 27% over forest and 13% over grassland. This improvement is consistent with expected smaller instrumental errors on evaporation during dry conditions [36]. Large positive incoming radiation anomalies (+221 W m^{-2}) reflect low cloud cover typical for anticyclones [6,13]. The increase in available energy is larger over forest than over grassland, mainly due to changes in longwave radiation. Albedo changes have limited impact [41]. The change in partitioning over forest and grassland diverges strongly (Fig. 1c,d). During the transition from wet to dry soil moisture conditions typical for HWDs, different stages can be distinguished, reflecting the nonlinear relationship between soil moisture and evapotranspiration (ET) [31,42,24,43]: (1) Stage I drying during which ET is independent of soil moisture [44,31], (2) Stage II drying during which ET becomes self-limiting [29,44], and (3) Stage III during which ET becomes negligible [31]. Note that the latent heat flux λET and ET relate via the latent heat of vaporization λ. Our analysis reveals that the additional energy over grassland (+136 W m^{-2}) is primarily used for evaporation of water (+83 W m^{-2}), rather than increasing sensible heating (+12 W m^{-2}). The average decrease in Bowen ratio (the ratio H/λET between sensible and latent heat flux) from 0.54 to 0.41 indicates stage I rather than stage II drying [44]. By contrast, forest maintains similar λET (+9 W m^{-2}) but uses the additional energy (+179 W m^{-2}) to effectively double H (+121 W m^{-2}), thereby increasing the Bowen ratio from 0.89 to 1.60. The median HWD anomalies for H and λET both differ significantly between forest (n=231) and grass-/cropland (n=210) sites (two-sided Wilcoxon rank sum test, $p<0.001$).

These results are consistent with previous findings around the German Hartheim site under cloudless conditions and ample supply of soil moisture [30]. Given the deeper roots of forest ecosystems [45,27,46], this increase should be attributed to the differential response of stomatal opening to radiation and atmospheric boundary layer feedbacks with temperature and humidity [24,21,25] (see Supplementary Figure 2), rather than soil moisture. In addition, the rough surface of forest canopies provides a more efficient turbulent heat exchange with the boundary layer [21,30,20,47], such that convective cooling relaxes the need for strong evaporative cooling during HWD conditions. The energy balance constraint is reflected in the distinct clustering of HWD anomalies of H and λET for forest and grassland sites, and also in the median HWD anomalies for the individual stations (Fig. 1c and Supplementary Figure 3). The scatter originates from random errors, daily variation in atmospheric conditions during HWDs, and from errors in estimating the baseline condition from limited data (contribution 20–30 W m^{-2}, see Methods and Supplementary Figure 4).

The contrasting Bowen ratio response can lead to dramatic energy budget differences at small spatial scales with a common atmospheric forcing. Figure 2 shows the diurnal cycle of the key elements of the land energy budget at the peak of the 2006 heatwave for three pairs of neighbouring flux towers over forest and grassland. While all sites experienced nearly cloud-free conditions, the maximum net radiation anomaly over the forested sites exceeds that of the grassland sites by 90–132 W m^{-2}. Combined with the Bowen ratio response, this results in a situation where the maximum heating of the atmosphere is up to four times larger at the forested sites than at grassland sites (420 versus 100 W m^{-2}, respectively, at the Dutch Cabauw and Loobos sites). Thus, forests literally appear to be "hot-spots" during the analysed summer heatwave conditions in Europe. In spite of the low soil moisture levels at all sites (see Supplementary Figure 5), the strong positive response of λET over grassland indicates stage I drying. Unfortunately, no flux observations are available over short vegetation in the low parts of Central France during the August 2003 extreme where large soil moisture depletion likely induced stage II drying [48,9,8].

Impact on land surface temperature

To diagnose flux partitioning across heatwave scenes of various intensities, including the August 2003 extreme, we employ satellite observations of land surface temperature (LST). The Moderate Resolution Imaging Spectroradiometer (MODIS) aboard the Terra and Aqua platforms provides sufficient spatial detail (30’’) to distinguish between main land use variations; moreover its records are long enough to determine anomalies (see Methods). Figure 3 shows the distribution of LST anomalies for pixels consisting predominantly (>67%) of grassland or forest during three HWD scenes. The scenes have been selected based on land cover mixture, absence of cloud cover and absence of strong regional LST gradients. The strong diurnal cycle of the LST anomalies confirms the key role of daytime heating on maximum temperatures. While for the July 2003 and July 2006 scenes the LST anomalies for grassland and forest are similar (Fig. 3a,b), they deviate during the peak of the August 2003 heatwave in Central France (Fig. 3c). The higher daytime anomalies over grassland are consistent with previous findings [8] and indicate a phase transition over grassland in this region towards a state with increased heating and temperatures. Note that Figures 3a,b reflect stage I drying while the increased temperature anomalies in Figure 3c indicate stage II/III drying over grassland.

Preferred states in heating and air temperature

We explore the potential for a phase transition during extended heatwave duration with a conceptual model that includes differences observed during stage I drying (Fig. 1) and is consistent with independent observations of stage II and III drying (see Methods). Figure 4a illustrates the typical non-linear relationships between soil moisture storage and ET, with a sharp drop in ET at low storage [42,24]. The nonlinearity is confirmed by observations from the Swiss Oensingen grassland site, one of the sites where the impact of the August 2003 heatwave was strongest, with λET dropping to 31% of the HWD median at low soil moisture. Soil moisture depletion at the German Wetzstein forest site was not sufficient to induce sensitivity to soil moisture. Figures 4b,c show the effect of the nonlinearity on the dynamics of λET and H during a hypothetical continuous drydown. For grassland, increased λET combines with the effect of shallower roots to expedite the onset of stage II drying to occur within the duration of the 2003 extreme as shown by the Oensingen data [6,1]. The onset of stage II drying can be regarded as a critical transition during which the system rapidly changes from a meta stable state (stage I) characterised by suppressed sensible heating to a stable state in which heating triples and becomes limited only by the available energy and ET is negligible (stage III). In absence of rain, this transition can occur in approximately a week's time [29]. It represents a crossing point where grassland surpasses forest as the major source of heating for the atmosphere. Over forest, H is less dynamic and almost insensitive to changes in λET [49]. A second crossing point exists due to the larger net radiation over forest.

The existence of two preferred states in the sensible heat flux can induce different modes in the regional temperature distribution. Figure 5 shows the evolution and distribution of the daily maximum temperature anomalies at six meteorological stations in the centre of the 2003 and 2006 heatwaves. In 2003, the extreme temperatures in France (exceeding 40°C) were only reached in August after a dry and warm summer with soil moisture depletion exceeding 2006 levels [48,50]. In 2003, dry conditions already started in May [48], while in 2006 the drought period was restricted to July and too short to cause widespread stage II drying. Although the monthly average daily maximum temperature anomaly in July 2006 exceeded that of August 2003 [9], maximum temperature anomalies on individual HWDs were smaller. To identify the preferred modes we fit a mixture of two Gaussian densities to the daily maximum temperature anomalies. In both cases the modes can be attributed to climatological (≈0 K) and heatwave conditions (>+5 K). The average heatwave mode for 2003 exceeds that of 2006 (+12.5 K vs. +7.1 K, respectively), which is consistent with the phase transition induced by the larger soil moisture depletion in 2003.

In conclusion, the most striking result of our study is that initially, the increase in sensible heat flux during HWDs is much larger over forest than over grassland. In the long term, however, elevated transpiration expedites soil moisture depletion, and grassland rather than forest becomes the major heat source. The regional climate system then shifts to a new regime characterized by a larger heating and even higher temperatures, such as during the catastrophic 2003 heatwave in France. By focusing strictly on the event timescale we could identify patterns that did not emerge in previous analyses on longer timescales [9,14,10]. Our results also highlight the dual role of forest in the terrestrial energy and water budgets: on the one hand the conservative character of forest evapotranspiration [28,21] accommodates higher sensible heat fluxes during HWDs, but on the other hand low losses are beneficial for water resources and prevent heatwave amplification in the long run. Such tradeoffs will become increasingly important in a warming climate.

Methods

HWD definition The World Meteorological Organization (WMO) defines a heatwave day (HWD) as a day in a sequence of at least 5 days during which the daily maximum temperature exceeds the climatological mean over the reference period 1961–1990 by at least 5 K. In this study we adopt the WMO definition but determine the climatology based on the available data in the period 1997–2008. Because of the increasing temperature trend in Europe, our method will generally result in fewer HWDs.

Flux measurements Concomitant observations of land surface radiation, energy, and water budget components come from the La Thuile FLUXNET synthesis dataset (www.fluxdata.org). This dataset provides direct and continuous eddy covariance flux measurements for over 170 sites across different climate and vegetation zones. For this study, only data were used from sites within the temperate climate zone of Central and Western Europe and with at least two (for climatology) or three (for anomalies) years of data. Gap-filled data and days with rain between 9:00 and 13:00 UTC were omitted from the analysis. In the analysis we distinguished between forested sites and sites with short (perennial) vegetation. Grassland and cropland sites were found to respond similarly to heatwave conditions.

Temperature measurements Station data displayed in Figure 5 were taken from the European Climate Analysis & Dataset (eca.knmi.nl).

Satellite data Daily quality-screened Moderate Resolution Imaging Spectroradiometer (MODIS) Collection 5 Land Surface Temperature (LST) at 1 km (MOD11A1 from TERRA and MYD11A1 from AQUA) were regridded to 0.1° by use of the following procedure: 1) Pixels with cloud, aerosol or cloud shadow artefacts (screening by QA bits 0 and 1) were excluded 2) Weighted averaging to a 0.1° regular grid was performed by weighting by the inverse of the LST error (evaluation of QA bits 6 and 7). The resulting spatiotemporal composite includes the 10–25 % most reliable clear sky pixels for the given area with four daily time steps. MODIS LST anomalies were calculated with respect to cloud-free conditions over a 15-day period centred on the day of interest for the years 2000–2008 (Terra) or 2003–2008 (Aqua) but excluding 2003 and July 2006.

Anomaly calculation When studying climate variability, it is useful to isolate the dynamic effects in a variable $\mathbf{X}$ from those imposed by the mean seasonal cycle: $\Delta\mathbf{X} = \mathbf{X} - \mathbf{X}_{\mathrm{clim}}$. The uncertainty associated with the anomaly $\Delta\mathbf{X}$ can be written as: $\sigma^2_{\Delta\mathbf{X}} = \sigma^2_{\mathbf{X}} + \sigma^2_{\mathbf{X}\mathrm{clim}} - 2\rho\sigma_{\mathbf{X}}\,\sigma_{\mathbf{X}\mathrm{clim}}$. When $\Delta\mathbf{X}$ can be estimated from all data within the defined climatology period (i.e., no gaps), $\sigma^2_{\mathbf{X}}$ will dominate $\sigma^2_{\mathbf{X}\mathrm{clim}}$. On the other hand when estimating $\mathbf{X}_{\mathrm{clim}}$ from a sample of the whole population, then $\sigma^2_{\mathbf{X}\mathrm{clim}} >> \sigma^2_{\mathbf{X}}$ and to a good approximation $\sigma^2_{\Delta\mathbf{X}} \approx \sigma^2_{\mathbf{X}\mathrm{clim}}$. We investigate the potential for estimating $\Delta\mathbf{X}$ from a limited sample of the whole population by applying a random combination method on gap-less data (see Supplementary Figure 4). This is relevant because different sites have different temporal coverage, and no single year can be defined as reference for all sites. Here find that by using at least 2 years of data and a 15-day window reduces $\sigma^2_{\Delta\mathbf{X}}$ sufficiently for practical applications.

Conceptual drydown model Key changes in the land surface energy budget during heatwaves are driven by changes in soil moisture. A three step model describes the impact of soil moisture on the sensible heat flux evolution. First we construct conceptual curves that relate storage and evapotranspiration. The levels of the curves during stage I drying (with no sensitivity to soil moisture storage depletion S) correspond to the median values listed in Figure 1 for the climatology (thin dashed lines in Fig. 4) and climatology plus HWD anomaly (thick lines). During stage II drying, ET becomes self-limiting and decays approximately exponentially[44,29]. The curves during stage II and III drying are constructed to be consistent with independent observations showing that (1) forest ecosystems have deeper roots [27,45,46] (25% deeper [45]) and (2) ET decays faster over grassland [29,31]. The conversion from the curves in Figure 3a to 3b is done using a simplified water budget without drainage and precipitation input, i.e. dS/dt = ET with a conversion between midday and daily ET of 0.3. Finally, the conversion from the curves in Figure 4B to 4C is done by assuming no change in available energy, i.e. λET + H = constant.

References

1. Schär, C. *et al.*, The role of increasing temperature variability for European summer heatwaves. *Nature* **427**, 332–336 (2004).
2. Seneviratne, S., Lüthi, D., Litschi, M. & Schär, C., Land-atmosphere coupling and climate change in Europe. *Nature* **443**, 205–209 (2006).
3. Fischer, E. & Schär, C., Consistent geographical patterns of changes in high-impact European heatwaves. *Nature Geosci.* **3**, 398–403 (2010).
4. Beniston, M., The 2003 heat wave in Europe: A shape of things to come? An analysis based on Swiss climatological data and model simulations. *Geophys. Res. Lett.* **31**, L02202 (2004).
5. Della-Marta, P., Haylock, M., Luterbacher, J. & Wanner, H., Doubled length of western European summer heat waves since 1880. *J. Geophys. Res.* **112** (D15), D15103 (2007).
6. Black, E. *et al.*, Factors contributing to the summer 2003 European heatwave. *Weather* **59** (8), 217–223 (2004).
7. García-Herrera, R. *et al.*, A review of the European summer heatwave of 2003. *Crit. Rev. Environ. Sci. Technol.* **40**, 267–306 (2010).
8. Zaitchik, B., Macalady, A., Bonneau, L. & Smith, R., Europe's 2003 heat wave: A satellite view of impacts and land-atmosphere feedbacks. *Int. J. Climatol.* **26**, 743–769 (2006).
9. Rebetez, M., Dupont, O. & Giroud, M., An analysis of the July 2006 heatwave extent in Europe compared to the record year of 2003. *Theor. Appl. Climatol.* **95** (1–2), 1–9 (2009).
10. Ciais, P. *et al.*, Europe-wide reduction in primary productivity caused by the heat and drought in 2003. *Science* **437**, 529–533 (2005).
11. Fischer, E., Seneviratne, S., Lüthi, D. & Schär, C., Contribution of land-atmosphere coupling to recent European summer heat waves. *Geophys. Res. Lett.* **34** (6), L06707 (2007).
12. Fouillet, A. *et al.*, Has the impact of heat waves on mortality changed in France since the

European heat wave of summer 2003? A study of the 2006 heat wave. *Int. J. Epidemiol.* **37** (2), 309–317 (2008).

13. Cassou, C., Terray, L. & Phillips, A., Tropical Atlantic influence on European heat waves. *J. Climate* **18**, 2805–2811 (2005).

14. Ferranti, F. & Viterbo, P., The European summer of 2003: Sensitivity to soil water initial conditions. *J. Climate* **19**, 3659–3680 (2006).

15. Shukla, J., Nobre, C. & Sellers, P., Amazon deforestation and climate change. *Science* **247** (4948), 1322–1325 (1990).

16. Wang, J. *et al.*, Impact of deforestation in the Amazon basin on cloud climatology. *Proc. Natl. Ac. Sci. USA* **106** (10), 3670–3674 (2009).

17. Bonan, G., Forests and climate change: Forcings, feedbacks, and the climate benefits of forests. *Science* **320**, 1444–1449 (2008).

18. Pitman, A. *et al.*, Uncertainties in climate responses to past land cover change: First results from the LUCID intercomparison study. *Geophys. Res. Lett.* **36**, L14814 (2009).

19. Jackson, R. *et al.*, Protecting climate with forests. *Environ. Res. Lett.* **3**, 044006 (2008).

20. Anderson, R. *et al.*, Biophysical considerations in forestry for climate protection. *Front. Ecol. Environ.*, doi:10.1890/090179 (2010).

21. Shuttleworth, J. & Calder, I., Has the Priestley-Taylor equation any relevance to forest evaporation? *J. Appl. Meteorol.* **18** (5), 639–646 (1979).

22. Zhang, L., Dawes, W. & Walker, G., Response of mean annual evapotranspiration to vegetation changes at catchment scale. *Water Resour. Res.* **37** (3), 701–708 (2001).

23. Hetherington, A. & Woodward, F., The role of stomata in sensing and driving environmental change. *Nature* **424** (6951), 901–908 (2003).

24. Kelliher, F., Leuning, R. & Schulze, E., Evaporation and canopy characteristics of coniferous forests and grasslands. *Oecologia* **95** (2), 153–163 (1993).

25. Jarvis, P. & McNaughton, K., Stomatal control of transpiration - Scaling up from leaf to region. *Adv. Ecol. Res.* **15**, 1–49 (1986).

26. Granier, A., Biron, P. & Lemoine, D., Water balance, transpiration and canopy conductance in two beech stands. *Agr. Forest Meteorol.* **100** (4), 291–308 (2000).

27. Schenk, H. & Jackson, R., The global biogeography of roots. *Ecol. Monogr.* **72** (3), 311–328 (2002).

28. Roberts, J., Forest transpiration: a conservative hydrological process? *J. Hydrol.* **66**, 133–141 (1983).

29. Teuling, A., Seneviratne, S., Williams, C. & Troch, P., Observed timescales of evapotranspiration response to soil moisture. *Geophys. Res. Lett.* **33** (23), L23403 (2006).

30. Wicke, W. & Bernhofer, C., Energy balance comparison of the Hartheim forest and an adjacent grassland site during the HartX experiment. *Theor. Appl. Climatol.* **53**, 49–58 (1996).

31. Baldocchi, D., Xu, L. & Kiang, N., How plant functional-type, weather, seasonal drought, and soil physical properties alter water and energy fluxes of an oak-grass savanna and an annual grassland. *Agr. Forest Meteorol.* **123**, 13–39 (2004).

32. von Randow, C. *et al.*, Comparative measurements and seasonal variations in energy and carbon exchange over forest and pasture in South West Amazonia. *Theor. Appl. Climatol.* **78**, 5–26 (2004).

33. Baldocchi, D. *et al.*, FLUXNET: A new tool to study the temporal and spatial variability of ecosystem-scale carbon dioxide, water vapor, and energy flux densities. *Bull. Am. Meteorol. Soc.* **82** (11), 2415–2434 (2001).

34. Wilson, K. *et al.*, Energy balance closure at FLUXNET sites. *Agr. Forest Meteorol.* **113**, 223–243 (2002).

35. Moderow, U. *et al.*, Available energy and energy balance closure at four coniferous forest sites across Europe. *Theor. Appl. Climatol.* **98**, 397–412 (2009).

36. Ibrom, A. *et al.*, Strong low-pass filtering effects on water vapour flux measurements with closed-path eddy correlation systems. *Agr. Forest Meteorol.* **147**, 140–156 (2007).

37. Foken, T. *et al.*, Some aspects of the energy balance closure problem. *Atmos. Chem. Phys.* **6**, 4395–4402 (2006).

38. Gash, J. & Dolman, A., Sonic anemometer (co)sine response and flux measurement I. The potential for (co)sine error to affect sonic anemometer-based flux measurements. *Agr. Forest. Meteorol.* **119**, 195–207 (2003).

39. Lindroth, A., Mölder, M. & Lagergren, F., Heat storage in forest biomass improves energy balance closure. *Biogeosciences* **7**, 301–313 (2010).

40. van der Molen, M., Gash, J. & Elbers, J., Sonic anemometer (co)sine response and flux measurement II. The effect of introducing an angle of attack dependent calibration. *Agr. Forest Meteorol.* **122**, 95–109 (2004).

41. Teuling, A. & Seneviratne, S., Contrasting spectral changes limit albedo impact on land-atmosphere coupling during the 2003 European heat wave. *Geophys. Res. Lett.* **35**, L03401

(2008).

42. Teuling, A., Uijlenhoet, R., Hupet, F. & Troch, P., Impact of plant water uptake strategy on soil moisture and evapotranspiration dynamics during drydown. *Geophys. Res. Lett.* **33** (3), L03401 (2006).

43. Seneviratne, S. *et al.*, Investigating soil moisture-climate interactions in a changing climate: A review. *Earth-Sci. Rev.* **99**, 125–161 (2010).

44. Brutsaert, W. & Chen, D., Desorption and the two stages of drying of natural tallgrass prairie. *Water Resour. Res.* **31** (5), 1305–1313 (1995).

45. Zeng, X., Global vegetation root distribution for land modeling. *J. Hydrometeor.* **2**, 525–530 (2001).

46. Breuer, L., Eckhardt, K. & Frede, H.-G., Plant parameter values for models in temperate climates. *Ecol. Model.* **169**, 237–293 (2003).

47. Juang, J.-Y. *et al.*, Separating the effects of albedo from eco-physiological changes on surface temperature along a successional chronosequence in the southeastern United States. *Geophys. Res. Lett.* **34**, L21408 (2007).

48. Andersen, O., Seneviratne, S., Hinderer, J. & Viterbo, P., GRACE-derived terrestrial water storage depletion associated with the 2003 European heat wave. *Geophys. Res. Lett.* **32**, L18405 (2005).

49. Wilson, K. *et al.*, Energy partitioning between latent and sensible heat flux during the warm season at FLUXNET sites. *Water Resour. Res.* **38** (12), 1294 (2002).

50. Seitza, F., Schmidt, M. & Shum, C., Signals of extreme weather conditions in Central Europe in GRACE 4-D hydrological mass variations. *Earth Planet. Sc. Lett.* **268**, 165–170 (2008).

Acknowledgements

This work used eddy covariance data acquired by the FLUXNET community and in particular by the CarboEuropeIP network. We acknowledge the financial support to the eddy covariance data harmonization provided by CarboEuropeIP, FAO-GTOS-TCO, iLEAPS, Max Planck Institute for Biogeochemistry, National Science Foundation, University of Tuscia, Université Laval and Environment Canada and US Department of Energy and the database development and technical support from Berkeley Water Center, Lawrence Berkeley National Laboratory, Microsoft Research eScience, Oak Ridge National Laboratory, University of California - Berkeley, University of Virginia. AJT acknowledges financial support from Netherlands Organisation for Scientific Research (NWO) through Rubicon grant 825.07.009, ETH Zurich and the NFP61 DROUGHT-CH project.

Author contributions

AJT and SIS provided the framework and conceived the manuscript. All authors collaborated in the discussion of the results and writing.

Competing Financial Interests statement

The authors declare no competing financial interests.

Figure captions

Figure 1 | Radiation and energy exchange over forest and grassland. The balance of incoming (↓) and outgoing (↑) shortwave (SW) and longwave (LW) radiation determines the net radiation (R_n) available for latent (λET), sensible (H), and ground (G) heat fluxes. The residual ($\varepsilon = R_n - \lambda ET - H - G$) encompasses both missing balance terms and bias. **a**, Location of flux towers. Open markers indicate multi-year sites without HWD observations. **b**, Flux climatologies. **c**, HWD sensible and latent heat flux anomalies ΔH and $\Delta \lambda ET$ with single-component Gaussian density contours and site medians. **d**, HWD anomalies. Vertical lines indicate 95% confidence limits for medians determined by bootstrapping.

Figure 2 | Energy exchanges at the peak of the July 2006 heatwave for neighbouring flux towers over forest and grassland. a, Cabauw and Loobos (distance 60 km). **b**, Mehrstedt and Hainich (distance 26 km). **c**, Grillenburg and Tharandt (distance 4 km). Regions are indicated in Fig. 1. Solid lines indicate HWD values, dashed lines the baseline conditions in a normal year. Black: net radiation (R_n), blue: latent heat flux (λET), red: sensible heat flux (H).

Arrows indicate maximum anomalies Δ for λET (grassland sites, upper panels), H (forest sites, lower panels), and R_n. See Figure 1 for location of map insets.

Figure 3 | Impact of land cover on local land surface temperature anomalies during heatwaves. a, Onset of heatwave (July 2003). **b**, Normal heatwave (July 2006). **c**, Extreme heatwave (August 2003). Upper panels: Daytime LST anomaly distribution (Terra/MODIS, 0.1° resolution). Dark shading indicates cloud cover. Lower panels: Evolution of median temperature anomalies for selected regions (1.4×2.4°) based on the high-resolution (30'') data. Vertical lines indicate 25th and 75th percentiles. Data have been observed with MODIS aboard the Terra (squares, overpass 9:30/21:30 h local solar time) and Aqua (circles, overpass 01:30/13:30 h) satellites. Splines were used for interpolation.

Figure 4 | Conceptual model for flux evolution over grassland and forest during drydown. See Methods for details. **a**, Relation between soil moisture storage depletion and midday latent heat flux λET. **b**, Temporal evolution of λET. **c**, Temporal evolution of sensible heat flux H. Values for λET and H during stage I drying are taken from Fig. 1, with dashed lines corresponding to the hypothetical situation of drydown under average conditions and thick lines corresponding to climatologies plus HWD anomalies. Points indicate independent observations of λET and soil moisture for Oensingen (grassland) and Wetzstein (forest) for HWDs in 2003 and July 2006.

Figure 5 | Screen-level daily maximum temperature anomaly evolution and distribution during heatwaves. Observations are made over grassland at meteorological stations. **a**, Paris, Bourges, Vichy (2003). **b**, De Bilt, Luxembourg, Berlin (2006). Thick lines represent 5-day moving averages. Circles indicate the means of individual components obtained by fitting a mixture of two Gaussian densities. Data are taken from the European Climate

Assessment & Dataset. Temperature anomalies over forest will differ less between 2003 and 2006 than those measured over grassland (Fig. 3). Arrows in **a** indicate the possible drydown stages during the summer of 2003.

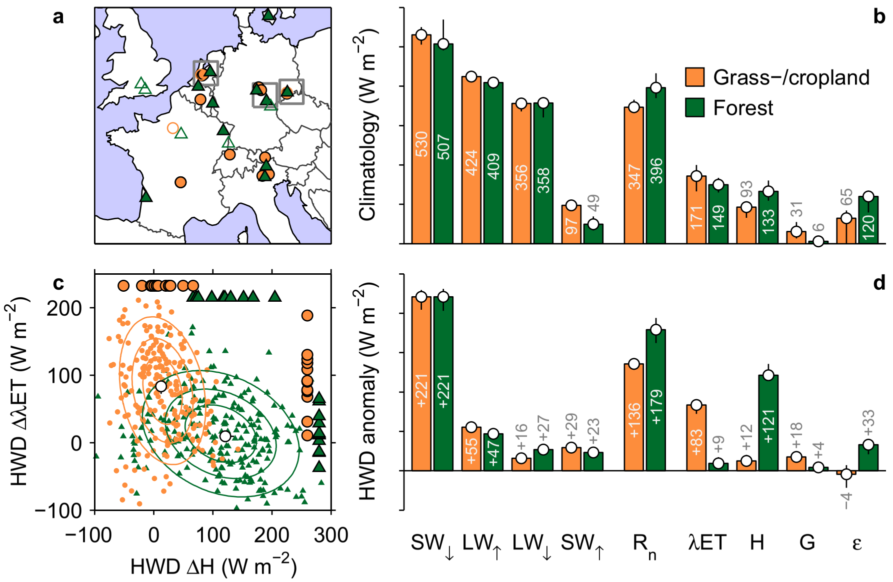
a
b
c
d
Climatology (W m^{-2})
Grass−/cropland
Forest
530
507
424
409
356
358
97
49
347
396
171
149
93
133
31
6
65
120
HWD anomaly (W m^{-2})
+221
+221
+55
+47
+16
+27
+29
+23
+136
+179
+83
+9
+12
+121
+18
+4
−4
+33
SW$_\downarrow$
LW$_\uparrow$
LW$_\downarrow$
SW$_\uparrow$
R$_n$
λET
H
G
ε
HWD ΔλET (W m^{-2})
HWD ΔH (W m^{-2})
200
100
0
−100
−100
0
100
200
300

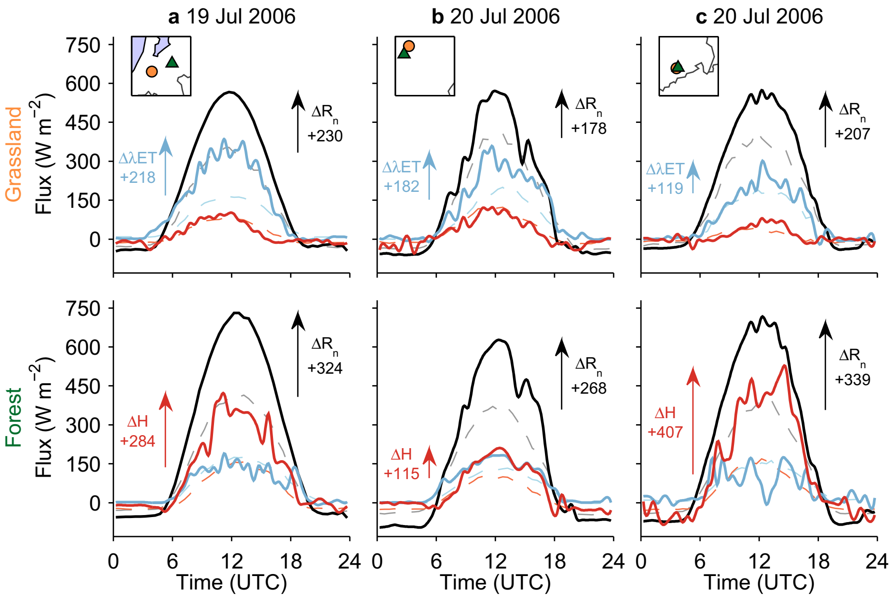

a 19 Jul 2006
b 20 Jul 2006
c 20 Jul 2006
Grassland
Forest
Flux (W m^{-2})
750
600
450
300
150
0
ΔR$_n$ +230
ΔλET +218
ΔR$_n$ +178
ΔλET +182
ΔR$_n$ +207
ΔλET +119
ΔR$_n$ +324
ΔH +284
ΔR$_n$ +268
ΔH +115
ΔR$_n$ +339
ΔH +407
0
6
12
18
24
Time (UTC)

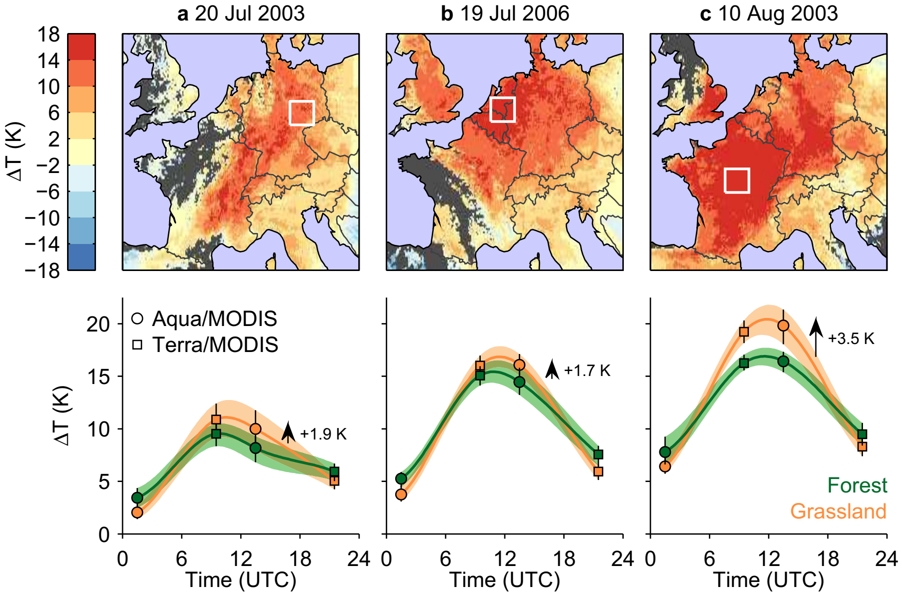

a 20 Jul 2003
b 19 Jul 2006
c 10 Aug 2003
18
14
10
6
2
−2
−6
−10
−14
−18
ΔT (K)
Aqua/MODIS
Terra/MODIS
20
15
10
5
0
ΔT (K)
+1.9 K
+1.7 K
+3.5 K
Forest
Grassland
0
6
12
18
24
Time (UTC)

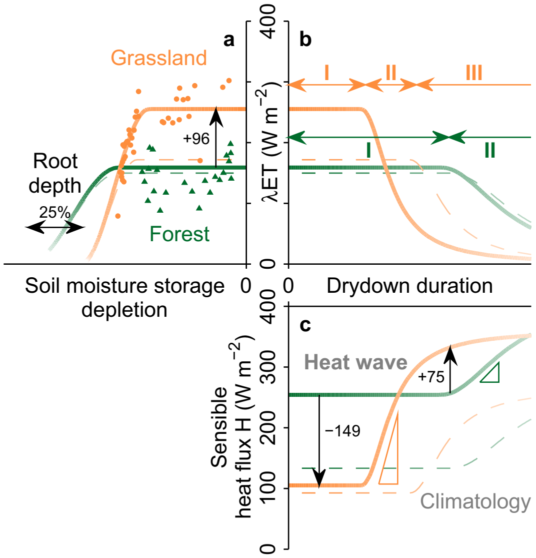
a
Grassland
+96
Root
depth
25%
Forest
Soil moisture storage
depletion
0
b
λET (W m^{-2})
400
0
I
II
III
I
II
0
Drydown duration
c
Sensible
heat flux H (W m^{-2})
400
300
200
100
0
Heat wave
+75
−149
Climatology

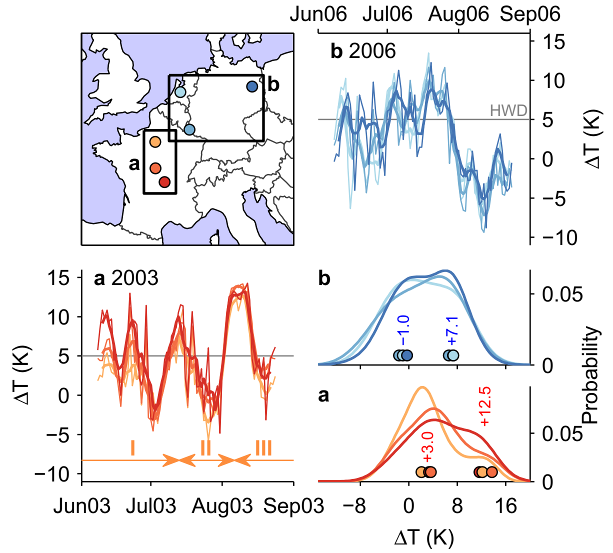
Jun06
Jul06
Aug06
Sep06
b 2006
HWD
ΔT (K)
15
10
5
0
−5
−10
b
a
a 2003
I
II
III
Jun03
Jul03
Aug03
Sep03
−1.0
+7.1
+3.0
+12.5
0.05
0
Probability
−8
0
8
16
ΔT (K)